Advances in Water Resources 71 (2014) 55–64

Contents lists available at ScienceDirect

Advances in Water Resources

journal homepage: www.elsevier.com/locate/advwatres

Forecast-skill-based simulation of streamflow forecasts

Tongtiegang Zhao, Jianshi Zhao *

State Key Laboratory of Hydro-Science and Engineering, Department of Hydraulic Engineering, Tsinghua University, Beijing, China

ARTICLE INFO

Article history:
Received 17 July 2013
Received in revised form 20 January 2014
Accepted 22 May 2014
Available online 29 May 2014

Keywords:
Streamflow variability
Forecast uncertainty
Forecast skill
Synthetic streamflow generation
Synthetic forecast generation

ABSTRACT

Streamflow forecasts are updated periodically in real time, thereby facilitating forecast evolution. This study proposes a forecast-skill-based model of forecast evolution that is able to simulate dynamically updated streamflow forecasts. The proposed model applies stochastic models that deal with streamflow variability to generate streamflow scenarios, which represent cases without forecast skill of future streamflow. The model then employs a coefficient of prediction to determine forecast skill and to quantify the streamflow variability ratio explained by the forecast. By updating the coefficients of prediction periodically, the model efficiently captures the evolution of streamflow forecast. Simulated forecast uncertainty increases with increasing lead time; and simulated uncertainty during a specific future period decreases over time. We combine the statistical model with an optimization model and design a hypothetical case study of reservoir operation. The results indicate the significance of forecast skill in forecast-based reservoir operation. Shortage index reduces as forecast skill increases and ensemble forecast outperforms deterministic forecast at a similar forecast skill level. Moreover, an effective forecast horizon exists beyond which more forecast information does not contribute to reservoir operation and higher forecast skill results in longer effective forecast horizon. The results illustrate that the statistical model is efficient in simulating forecast evolution and facilitates analysis of forecast-based decision making.

1. Introduction

Water resource system analysis faces the problem of unknown future streamflow [17,21,26]. Conventionally, future streamflow conditions are represented by streamflow variability and stochastic models are developed for synthetic streamflow generation. Streamflow sequences that contain statistical properties similar to those of historical streamflow data are generated and then applied to assist in water resource planning, e.g., reservoir capacity determination, storage yield analysis, and irrigation system design [15,18,25]. In recent years, streamflow forecasting has been improved considerably, which has provided useful information concerning future streamflow in real time. Meanwhile, streamflow forecasting has not yet been perfected and remains characterized by forecast uncertainty [11,23,34].

Streamflow variability and forecast uncertainty are two key issues in water resource studies [1,5,27]. Streamflow variability has been sufficiently addressed in stochastic hydrology. Parametric models (e.g., time series models) and nonparametric models (e.g., K-nearest neighbor models) are used in synthetic streamflow generation [6,30,33]. By contrast, only a few stochastic models are concerned with forecast uncertainty. Water resources studies illustrated that applications of streamflow forecasts lead to more economic benefits compared with conventional operating rules, which are considerably affected by forecast uncertainty [9,23,28]. Meanwhile, previous forecast-based decision making provides a limited number of samples, which causes difficulty in generalizing the relationship between economic benefit and forecast uncertainty. The use of stochastic models enables explicit characterization and simulation of forecast uncertainty and can bridge this gap [2,10,23]. Based on stochastic models that address streamflow variability, this study develops a stochastic model for simulating forecast uncertainty.

Combining stochastic models of forecast uncertainty with optimization models facilitates analysis of forecast-based decision making. For example, Maurer and Lettenmaier [22], Maurer and Lettenmaier [23] developed stochastic models of predictability and evaluated economic benefits from predictability of seasonal streamflow. Georgakakos and Graham [10] and Graham and Georgakakos [12] assessed the benefits of streamflow forecasts and illustrated that the use of forecast is affected by characteristics of reservoir systems. Zhao et al. [37,39] constructed models of the evolution of streamflow forecasts and evaluated the effects of

* Corresponding author. Tel.: +86 10 62796539; fax: +86 10 62796971.
E-mail address: zhaojianshi@tsinghua.edu.cn (J. Zhao).

http://dx.doi.org/10.1016/j.advwatres.2014.05.011
0309-1708/

Gaussian and non-Gaussian forecast uncertainties on reservoir operation. These studies are based on parametric stochastic models for which the statistical distributions and a number of related parameters should be specified. Using parametric models, we develop a forecast-skill-based model of forecast evolution (FMFE) with three advantageous properties. First, the model is based on forecast skill, which is a key metric for forecast evaluation that can be derived from previous forecasts. Second, the model is nonparametric and does not involve tedious statistical specifications, e.g., mean, variance, and covariance. Third, the model takes full advantage of stochastic models, which are used in synthetic streamflow generation.

In the remainder of the paper, Section 2 presents a brief summary of the parametric models used to simulate streamflow forecasts. Section 3 details the nonparametric FMFE model and examines the properties of simulated forecast uncertainty. Section 4 demonstrates an application of the model to simulation of streamflow forecast. Section 5 presents a decision making analysis and illustrates effect of forecast skill on forecast-based reservoir operation. Section 6 provides the discussions and conclusions.

2. Simulation of streamflow forecast

Using time indices s and t, and denoting $f_{s,t}$ as the forecast of streamflow q_t that is made at period s, and the forecast horizon as H, the forecasts made at period s form a forecast vector:

$$F_{s,-} = [f_{s,s} \quad f_{s,s+1} \quad f_{s,s+2} \quad \dots \quad f_{s,s+H}] \tag{1}$$

$H+1$ forecasts are made at period s. Moreover, $H+1$ forecasts correspond to q_t made during the preceding periods $t-H, t-H+1, \dots$, and $t-1$, as well as period t, form the following vector:

$$F_{-,t} = [f_{t-H,t} \quad f_{t-H+1,t} \quad f_{t-H+2,t} \quad \dots \quad f_{t,t}] \tag{2}$$

$F_{s,-}$ and $F_{-,t}$ are differentiated in Eqs. (1) and (2), respectively. We present a brief summary of the stochastic models used in the simulation of streamflow forecasts.

2.1. Simulation of forecasts made in one period

Forecast uncertainty can generally be indicated by the gap between forecast $f_{s,t}$ and the real value of streamflow q_t [20,28,35]. In the deterministic case, forecast uncertainty is represented by forecast error $e_{s,t}$,

$$e_{s,t} = f_{s,t} - q_t \tag{3}$$

Following Eqs. (1) and (3), the uncertainty of the streamflow forecasts generated during period s is characterized by the following vector:

$$E_{s,-} = [e_{s,s} \quad e_{s,s+1} \quad e_{s,s+2} \quad \dots \quad e_{s,s+H}] \tag{4}$$

For the fixed period s, the forecast uncertainty in $f_{s,t}$ tends to increase with t, i.e., a longer lead time leads to increased uncertainty [22,23], as shown in Fig. 1.

For the sake of simplicity, the stochastic models of forecast uncertainty can assume that $e_{s,s+i}$ ($i = 0,1,2,\dots,H$) are mutually independent, which allows for the independent simulation of $e_{s,s+i}$. The assumption of Gaussian distribution leads to the following [23]:

$$e_{s,s+i} \sim N(m_i, \sigma_i^2) \quad (i = 0, 1, 2, \dots, H) \tag{5}$$

In Eq. (5), m_i and σ_i^2 are the mean and variance of $e_{s,s+i}$, respectively. Thus, $e_{s,s+i}$ is simulated by:

$$e_{s,s+i} = m_i + \sigma_i \varepsilon_i \tag{6}$$

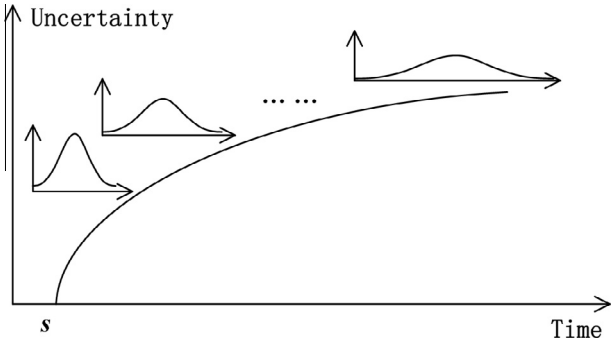

Fig. 1. Longer forecast lead time leads to greater forecast uncertainty.

In Eq. (6), ε_i is a standard Gaussian random number, i.e., $\varepsilon_i \sim N(0, 1^2)$. Other statistical distributions, e.g., log-Gaussian distribution and Gamma distribution, have also been used to simulate forecast uncertainty [12,28].

The variance σ_i^2 of $e_{s,s+i}$ (Eq. (5)) has often been used as an indicator of the magnitude of forecast uncertainty [19,35,36]. In simulations of single-period forecast uncertainties, the variance is usually set as:

$$\sigma_0^2 \leqslant \sigma_1^2 \leqslant \sigma_2^2 \leqslant \cdots \leqslant \sigma_H^2 \tag{7}$$

This equation indicates the characteristic longer lead time induces greater forecast uncertainty. The variance is also set as:

$$\sigma_H^2 \leqslant \mathrm{var}(q_{s+H}) \tag{8}$$

where $\mathrm{var}(q_{s+H})$ indicates streamflow variability within time period $s+H$. This equation implies that the magnitude of forecast uncertainty cannot be greater than that of streamflow variability. Otherwise, having no forecast would be a better option [23].

Comparison between forecast uncertainty and streamflow variability indicates the forecast skill. Denoting the variability of q_{s+i} ($i = 0,1,2,\dots,H$) as $\mathrm{var}(q_{s+i})$ and the uncertainty of the corresponding forecast $f_{s,s+i}$ as σ_i^2 ($i = 0,1,2,\dots,H$), the coefficient of prediction (C_p) measures the fraction of streamflow variability explained by the forecast [22,23,29], i.e.,

$$\sigma_i^2 = (1 - C_p)\mathrm{var}(q_{s+i}) \quad (i = 0, 1, \dots, H) \tag{9}$$

In Eq. (9), the case $C_p = 1$ represents perfect forecast skill, such that σ_i^2 becomes zero; the case $C_p = 0$ stands for no forecast skill, such that $\sigma_i^2 = \mathrm{var}(q_{s+i})$. The phenomenon whereby C_p decreases with lead time implies that σ_i^2 increases with i, which indicates decreasing forecast skill and increasing uncertainty with increasing forecast lead time [23].

Eqs. (4)–(9) illustrate the simulation steps for independent forecast uncertainties. Incorporating the variance–covariance matrix $VCVE$ enables the simulation of correlated uncertainties [38], i.e.,

$$VCVE = \begin{pmatrix} \mathrm{ve}_0 & \mathrm{cove}_{0,1} & \mathrm{cove}_{0,2} & \cdots & \mathrm{cove}_{0,H} \\ \mathrm{cove}_{1,0} & \mathrm{ve}_1 & \mathrm{cove}_{1,2} & \cdots & \mathrm{cove}_{1,H} \\ \mathrm{cove}_{2,0} & \mathrm{cove}_{2,1} & \mathrm{ve}_2 & \cdots & \mathrm{cove}_{2,H} \\ \vdots & \vdots & \vdots & \ddots & \vdots \\ \mathrm{cove}_{H,0} & \mathrm{cove}_{H,1} & \mathrm{cove}_{H,2} & \cdots & \mathrm{ve}_H \end{pmatrix} \tag{10}$$

In Eq. (10), $\mathrm{cove}_{i,j}$ ($i, j = 0,1,2,\dots,H$) denotes the covariance of $e_{s,s+i}$ and $e_{s,s+j}$; ve_i is the variance of $e_{s,s+i}$, which is also denoted as σ_i^2 in Eq. (5). Variance–covariance matrices are semi-definite. Through Cholesky decomposition, $VCVE$ can be decomposed into the product of a matrix multiplied by its transpose, i.e.,

$$VCVE = VE^* VE^T \tag{11}$$

The correlated forecast uncertainty can be generated based on VE^T, i.e.,

$$[e_{s,s} \quad e_{s,s+1} \quad e_{s,s+2} \quad \dots \quad e_{s,s+H}] = [\varepsilon_0 \quad \varepsilon_1 \quad \varepsilon_2 \quad \dots \quad \varepsilon_H]^* VE^T \tag{12}$$

In Eq. (12), $[\varepsilon_0 \quad \varepsilon_1 \quad \varepsilon_2 \quad \cdots \quad \varepsilon_H]$ are $H+1$ independent and identically distributed standard Gaussian random numbers, and $[e_{s,s} \quad e_{s,s+1} \quad e_{s,s+2} \quad \cdots \quad e_{s,s+H}]$ are simulated forecast errors. According to Eqs. (10)–(12), the linear correlation between $e_{s,s+i}$ and $e_{s,s+j}$ is $\frac{\text{cove}_{ij}}{\sqrt{\text{ve}_i \times \text{ve}_j}}$.

2.2. Simulation of the evolution of streamflow forecasts

Eqs. (4)–(12) illustrate the simulation of the uncertainties $[e_{s,s} \quad e_{s,s+1} \quad e_{s,s+2} \quad \cdots \quad e_{s,s+H}]$ of forecast $[f_{s,s} \quad f_{s,s+1} \quad f_{s,s+2} \quad \cdots \quad f_{s,s+H}]$ in period s. In real-time cases, streamflow forecasts are updated periodically. At the beginning of one period, the streamflow forecast is made based on the available hydrological information. As time progresses, additional hydrological information becomes available and new forecasts are made in subsequent periods [9,19,28]. Dynamically updated forecasts represent a process of forecast evolution, as shown in Fig. 2. For streamflow q_t at specific future period t, the uncertainty in forecast $f_{s,t}$ generally decreases as time s progresses toward t.

As to q_t ($t = 1,2,\dots,T$), the evolution of the corresponding forecasts are embedded in the dynamically updated streamflow forecasts from Period 1 to T. When extending Eq. (10) to simulate the forecasts from Period 1 to T, T vectors comprise $T \times (H+1)$ forecast errors, as follows:

$$\begin{cases} E_{1,-} = [e_{1,1} \quad e_{1,1+1} \quad e_{1,1+2} \quad \dots \quad e_{1,1+H}] \\ E_{2,-} = [e_{2,2} \quad e_{2,2+1} \quad e_{2,2+2} \quad \dots \quad e_{2,2+H}] \\ \cdots \\ E_{T,-} = [e_{T,T} \quad e_{T,T+1} \quad e_{T,T+2} \quad \dots \quad e_{T,T+H}] \end{cases} \tag{13}$$

As a result, there are $[T \times (H+1)]^2$ parameters in the variance–covariance matrix in the simple case of unbiased Gaussian forecast uncertainty. For example, when $T = 30$ days and $H = 4$ days, $(30 \times 5)^2 = 22{,}500$ parameters exist in the variance–covariance matrix. Cases with biased and non-Gaussian uncertainties contain even more parameters.

Forecast errors can be decomposed into forecast improvements to circumvent the problem faced by the simulation of forecast errors [14,37,39]. Forecast improvement $u_{s,t}$ is defined as the reduction of the forecast error $e_{s,t}$ of period s from the error $e_{s-1,t}$ of the previous period $s-1$, error $e_{s-1,t}$, i.e.,

$$u_{s,t} = e_{s,t} - e_{s-1,t} = (f_{s,t} - q_t) - (f_{s-1,t} - q_t) = f_{s,t} - f_{s-1,t} \tag{14}$$

Based on Eq. (14), the following equation is derived:

$$\begin{cases} u_{t,t} = f_{t,t} - f_{t-1,t} \\ u_{t-1,t} = f_{t-1,t} - f_{t-2,t} \\ \cdots \\ u_{t-H+1,t} = f_{t-H+1,t} - f_{t-H,t} \end{cases} \tag{15}$$

which indicates that $u_{s,t}$ represents the improvement of the forecast $f_{s,t}$ in period s over the forecast $f_{s-1,t}$ of the previous period $s-1$, as shown in Fig. 3.

Forecast improvements made during period s form a vector $U_{s,-}$, i.e.,

$$U_{s,-} = [u_{s,s} \quad u_{s,s+1} \quad u_{s,s+2} \quad \dots \quad u_{s,s+H-1}] \tag{16}$$

Notably, $F_{s,-}$ and $E_{s,-}$ contain $H+1$ elements [Eqs. (1) and (4)], whereas $U_{s,-}$ consists of H elements because $f_{s,s+H}$ is a new forecast with the maximum lead time but without the corresponding forecast improvement. Forecast improvements $U_{s,-}$ result from updates in hydrological information, e.g., initial soil moisture conditions and precipitation forecasts. Hydrological information updates can generally be treated as independent. Otherwise, more future hydrological information can be inferred from the currently available information [37,39]. This condition facilitates the independent simulation of forecast improvement vectors $U_{s,-}$ ($s = 1,2,\dots,T$).

When $U_{s,-}$ follows unbiased Gaussian distribution, the former can be characterized by the variance–covariance matrix $VCVU$:

$$VCVU = \begin{pmatrix} \text{vu}_0 & \text{covu}_{0,1} & \text{covu}_{0,2} & \cdots & \text{covu}_{0,H-1} \\ \text{covu}_{1,0} & \text{vu}_1 & \text{covu}_{1,2} & \cdots & \text{covu}_{1,H-1} \\ \text{covu}_{2,0} & \text{covu}_{2,1} & \text{vu}_2 & \cdots & \text{covu}_{2,H-1} \\ \vdots & \vdots & \vdots & \ddots & \vdots \\ \text{covu}_{H-1,0} & \text{covu}_{H-1,1} & \text{covu}_{H-1,2} & \cdots & \text{vu}_{H-1} \end{pmatrix} \tag{17}$$

In Eq. (17), $\text{covu}_{i,j}$ ($i, j = 0,1,\dots,H-1$) denotes the covariance of $u_{s,s+i}$ and $u_{s,s+j}$, and vu_i is the variance of $u_{s,s+i}$. At the onset of the simulation of $U_{s,-}$, $VCVU$ is decomposed by means of Cholesky decomposition:

$$VCVU = VU^* VU^T \tag{18}$$

$U_{s,-}$ is then simulated by using VU^T, i.e.,

$$[u_{s,s} \quad u_{s,s+1} \quad u_{s,s+2} \quad \dots \quad u_{s,s+H-1}] = [\varepsilon_0 \quad \varepsilon_1 \quad \varepsilon_2 \quad \dots \quad \varepsilon_{H-1}]^* VU^T \tag{19}$$

In Eq. (19), $[\varepsilon_0 \quad \varepsilon_1 \quad \varepsilon_2 \quad \dots \quad \varepsilon_{H-1}]$ are H independent and identically distributed standard Gaussian random numbers, and $[u_{s,s} \quad u_{s,s+1} \quad u_{s,s+2} \quad \dots \quad u_{s,s+H-1}]$ are simulated forecast improvements. Eqs. (17)–(19) illustrate the simulation steps for unbiased Gaussian forecast uncertainty. Incorporating statistical methods that transform distributions of stochastic variables enables the simulation of biased and non-Gaussian forecast uncertainties [39]. For example, normal quantile transform (NQT) converts non-Gaussian variables into Gaussian variables, whereas inverse-NQT transforms Gaussian variables into non-Gaussian variables [16,24].

Based on synthetic forecast improvements, forecasts $[f_{t-H,t} \quad f_{t-H+1,t} \quad f_{t-H+2,t} \quad \dots \quad f_{t,t}]$ that correspond to q_t are simulated as follows:

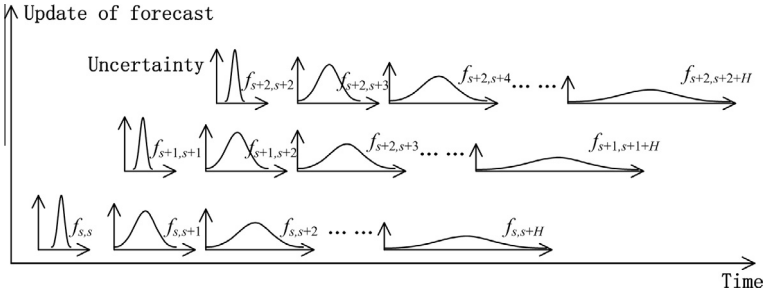

Fig. 2. Schematic of evolution of streamflow forecasts.

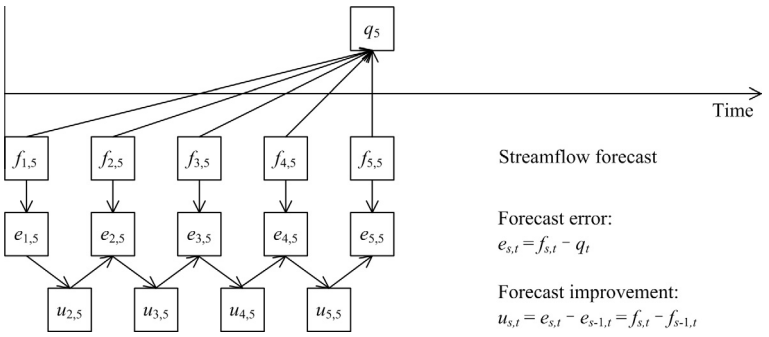

Fig. 3. Relationships among streamflow forecast, forecast error, and forecast improvement.

$$\begin{cases} f_{t,t} = q_t \\ f_{t-1,t} = q_t - u_{t,t} \\ f_{t-2,t} = q_t - u_{t,t} - u_{t-1,t} \\ \dots \\ f_{t-H,t} = q_t - u_{t,t} - u_{t-1,t} - \dots - u_{t-H+1,t} \end{cases} \tag{20}$$

This equation implies that:

$$\begin{cases} e_{t,t} = 0 \\ e_{t-1,t} = -u_{t,t} \\ e_{t-2,t} = -u_{t,t} - u_{t-1,t} \\ \dots \\ e_{t-H,t} = -u_{t,t} - u_{t-1,t} - \dots - u_{t-H+1,t} \end{cases} \tag{21}$$

In Eqs. (20) and (21), $f_{t,t} = q_t$, i.e., the forecast of the streamflow of the current period is perfect. Given that the forecast improvements at different periods are independently simulated, we have

$$\begin{cases} \mathrm{var}(e_{t,t}) = 0 \\ \mathrm{var}(e_{t-1,t}) = \mathrm{vu}_{0,0} \\ \mathrm{var}(e_{t-2,t}) = \mathrm{vu}_{0,0} + \mathrm{vu}_{1,1} \\ \dots \\ \mathrm{var}(e_{t-H,t}) = \mathrm{vu}_{0,0} + \mathrm{vu}_{1,1} + \dots + \mathrm{vu}_{H-1,H-1} \end{cases} \tag{22}$$

This equation demonstrates that as time s progresses toward t, the uncertainty of forecast $f_{s,t}$ decreases. Therefore, the decomposition approach (see Fig. 3) efficiently captures the evolution of uncertainty in dynamically updated streamflow forecasts.

We briefly summarize stochastic models for the simulation of streamflow forecasts in Eqs. (3)–(22). The parameters in *VCVE* [variance–covariance matrix of forecast errors, Eq. (10)] and *VCVU* [variance–covariance matrix of forecast improvements, Eq. (17)] have a central function [14,37,39]. As a result, the model application faces the tedious specification of parameters, particularly when the forecast horizon H is long. If forecast uncertainty follows biased and non-Gaussian distributions, then more parameters should be specified. The following section presents an efficient nonparametric model for simulating streamflow forecasts based on the preceding formulations of parametric stochastic models.

3. Forecast-skill-based model of forecast evolution

This section develops a nonparametric model for simulation of forecast evolution. Based on forecast skill, which is indicated by the coefficient of prediction (*CP*), the FMFE model extends stochastic models used for synthetic streamflow generation to synthetic forecast generation.

3.1. Forecast skill and forecast uncertainty

A large number of stochastic models have been developed to simulate streamflow variability (e.g., those proposed by [15,18,25], which focus on generating streamflow sequences similar to historical streamflow data in terms of statistical properties such as mean value, standard deviation, coefficient of skewness, and interdependence relationship [26]. Generally, synthetic streamflow sequences provide statistical information on future streamflow, which represents the case with no forecast skill. Using m as the index of streamflow sequence, we denote the streamflow sequences from Period 1 to T as:

$$[\,q_1^m \quad q_2^m \quad \dots \quad q_T^m\,] \quad (m = 1, 2, \dots, M) \tag{23}$$

where M is the total number of synthetic streamflow sequences. When forecast skill is perfect, the streamflow from Period 1 to T is perfectly known, i.e.,

$$[\,q_1 \quad q_2 \quad \dots \quad q_T\,] \tag{24}$$

Eqs. (23) and (24) illustrate two ideal cases without and with perfect forecast skills, respectively. Real-world streamflow forecasts lie in between these two cases. Although perfect forecast skill is difficult to obtain, streamflow forecast skills exist within a certain forecast horizon [19,28,35]. The gap between q_t^m and q_t is derived as follows:

$$e_t^m = q_t^m - q_t \quad (m = 1, 2, \dots, M) \tag{25}$$

where e_t^m $(m = 1,2,\dots,M)$ represents forecast uncertainty when there is no forecast skill of q_t.

We use a *CP* to quantify forecast skill. $CP_{s,t}$ denotes the forecast skill for q_t at period s, i.e., the fraction of error e_t^m reduced by forecast $f_{s,t}^m$ (m is the index of forecast scenarios in the ensemble forecast). Based on q_t, e_t^m, and $CP_{s,t}$, streamflow forecast $f_{s,t}^m$ is simulated as follows:

$$f_{s,t}^m = q_t + (1 - CP_{s,t})e_t^m = CP_{s,t}q_t + (1 - CP_{s,t})q_t^m \quad (m = 1, 2, \dots, M) \tag{26}$$

The simulated forecast uncertainty is

$$e_{s,t}^m = f_{s,t}^m - q_t = (1 - CP_{s,t})e_t^m \quad (m = 1, 2, \dots, M) \tag{27}$$

Given that $CP_{s,t}$ indicates forecast skill, in a case with perfect forecast skill, $CP_{s,t} = 1$, which makes $f_{s,t}^m = q_t$ and $e_{s,t}^m = 0$. Meanwhile, in a case without forecast skill, $CP_{s,t} = 0$, which makes $f_{s,t}^m = q_t^m$ and $e_{s,t}^m = e_t^m$. Eqs. (23)–(27) illustrate the simulation steps for streamflow forecasts based on synthetic streamflow sequences and pre-specified coefficients of prediction. The equations set up the framework of the FMFE model, which consists of three steps, as illustrated in Fig. 4.

The first step is the quantification of forecast skill. At period s, the forecast skill of streamflow in subsequent periods is

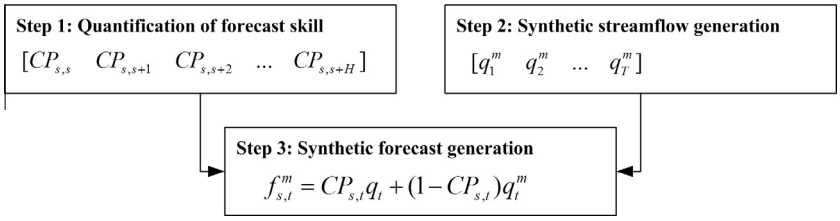

Fig. 4. Framework of the FMFE model.

represented by $CP_{s,s+i}$ ($i = 0,1,2,\ldots,H$). The value of $CP_{s,s+i}$ can be updated by using s, which indicates the updating of forecast skills over time and simulates forecast evolution.

The second step is synthetic streamflow generation. This step takes advantage of stochastic models simulating streamflow variability and involves the synthesis of a number of streamflow sequences to represent streamflow variability. Notably, streamflow variability can be derived from historical streamflow sequences [18,25,31] and also climate change projections [3,23,32].

The third step is synthetic forecast generation. The model extends the stochastic models of streamflow variability to the simulation of forecast uncertainty by incorporating forecast skills. Notably, the setting $M = 1$ simulates a deterministic streamflow forecast with a single forecast scenario, whereas the setting $M > 1$ simulates an ensemble forecast with multiple forecast scenarios.

3.2. Properties of simulated forecast uncertainty

The FMFE model provides a simple nonparametric approach to synthetic forecast generation based on stochastic models for synthetic streamflow generation. The simulated forecast uncertainty generally exhibits four key characteristics.

First, the statistical distribution of the simulated forecasts depends on the stochastic model dealing with streamflow variability. Eq. (26) is essentially a linear transformation of synthetic streamflow sequences. For two stochastic variables x and y, if $y = a \times x + b$ (a and b are two parameters of the linear transformation), then the statistical distributions of x and y are the same. Thus, the distribution of forecasts $f_{s,t}^m$ ($m = 1,2,\ldots,M$) of q_t, which are simulated by the FMFE model, is determined by the distribution of q_t^m ($m = 1,2,\ldots,M$), which is determined by the stochastic models for streamflow variability. In stochastic hydrology, stochastic models are used to simulate streamflow sequences following Gaussian, log-Gaussian, or other more complicated distributions (e.g., [6,26,30]). Thus, the FMFE model can simulate forecast uncertainty following different distributions by employing different stochastic models that synthesize streamflow.

Second, simulated streamflow forecasts are generally biased. The linear transformation $y = a \times x + b$ leads to the following:

$$\begin{cases} E(y) = a \times E(x) + b \\ Var(y) = a^2 \times Var(x) \end{cases} \tag{28}$$

where $E()$ and $Var()$ are the operators for expectation and variance, respectively. Considering that $f_{s,t}^m = q_t + (1 - CP_{s,t})(q_t^m - q_t)$, we derive the following:

$$E([f_{s,t}^1 \quad f_{s,t}^2 \quad \ldots \quad f_{s,t}^M]) = CP_{s,t} \times q_t + (1 - CP_{s,t}) \times E([q_t^1 \quad q_t^2 \quad \ldots \quad q_t^M]) \tag{29}$$

The preceding equation implies bias in the simulated forecasts, which indeed exists in real-world forecasts. For example, underestimation occurs in flood forecasts, and longer lead time results in larger underestimation of coming floods [39]. Eq. (29) suggests the existence of underestimation in simulated forecasts for high-flow events with streamflows larger than their mean values, and the existence of overestimation in simulated forecasts for low-flow events. Aside from the level of q_t and $E([q_t^1 \quad q_t^2 \quad \ldots \quad q_t^M])$, the bias of the simulated forecasts also depends on $CP_{s,t}$. When $CP_{s,t} = 1$, the forecasts are perfect and unbiased. As $CP_{s,t}$ decreases, under- or overestimation in the forecasts tends to increase.

Third, the indication of forecast skill by $CP_{s,t}$ is inversely related with the magnitude of forecast uncertainty. Based on Eq. (28), the following is derived:

$$Var([f_{s,t}^1 \quad f_{s,t}^2 \quad \ldots \quad f_{s,t}^M]) = (1 - CP_{s,t})^2 \times Var([q_t^1 \quad q_t^2 \quad \ldots \quad q_t^M]) \tag{30}$$

where $(1 - CP_{s,t})^2$ indicates the ratio of forecast uncertainty to streamflow variability. The coefficient of prediction [C_p, see Eq. (9)], originally proposed by Maurer and Lettenmaier [22,23], is the fraction of streamflow variability explained by streamflow forecast. The $CP_{s,t}$ proposed in our study is a modified version of C_p. As implied by Eq. (30), $1-(1 - CP_{s,t})^2$ represents the streamflow variability explained by the forecast. Thus, the relationship between C_p and $CP_{s,t}$ is:

$$1 - C_p = (1 - CP_{s,t})^2 \tag{31}$$

Therefore, for a given forecast model, after evaluating C_P at different lead times, we can derive $CP_{s,t}$ as:

$$CP_{s,t} = 1 - \sqrt{1 - C_p} \tag{32}$$

Based on $CP_{s,t}$, synthetic forecasts can be generated for the given forecast model. Given that previous forecasts provide limited samples of forecast uncertainty, applying the FMFE model facilitates a large number of samples to represent forecast uncertainty.

Fourth, dynamically updated streamflow forecasts can be simulated by updating $CP_{s,t}$ ($t = s, s+1,\ldots,s+H$) with s. For period s, the forecast skill of the streamflow in subsequent periods is indicated by the vector $CP_{s,-}$, i.e.,

$$CP_{s,-} = [CP_{s,s} \quad CP_{s,s+1} \quad CP_{s,s+2} \quad \ldots \quad CP_{s,s+H}] \tag{33}$$

Given that a longer lead time results in lower forecast skill, we have:

$$CP_{s,s} \geqslant CP_{s,s+1} \geqslant CP_{s,s+2} \geqslant \ldots \geqslant CP_{s,s+H} \tag{34}$$

Moreover, if $CP_{s,s+i}$ (i.e., forecast skill) depends on i (lead time) only and does not change with s, Eqs. (33) and (34) imply that

$$CP_{t,t-H} \leqslant CP_{t,t-H+1} \leqslant CP_{t,t-H+2} \leqslant \ldots \leqslant CP_{t,t} \tag{35}$$

The preceding equations indicate that forecast skill q_t improves as time progresses toward t.

To summarize, the FMFE model can simulate dynamically updated streamflow forecasts. The major advantage of the nonparametric model is its simplicity of use when handling the evolution of streamflow forecasts. Compared with parametric models that employ a number of parameters to specify characteristics, e.g., statistical distribution, mean, and variance, the proposed model characterizes and simulates forecast uncertainty based on a single sequence of coefficients of prediction.

4. Simulation of streamflow forecast

This section presents an application of the FMFE model to simulate streamflow forecast. The model comprises three steps. In step 1, $CP_{s,t}$ is set as 1 for the current period ($t = s$) and $CP_{s,t}$ decreases with lead time $t - s$ at a rate of δ until the value of $CP_{s,t}$ reaches 0. Thus, $CP_{s,t}$ is,

$$CP_{s,t} = \max(1 - \delta(t - s), 0) \tag{36}$$

Notably, in Eq. (36), for fixed period s, $CP_{s,t}$ decreases as t increases, resulting in a lower forecast skill at a longer lead time; for a given t, $CP_{s,t}$ increases as s increases, indicating improvement of forecast skill as time progresses; and for a certain lead time $t - s$, a larger δ results in a smaller $CP_{s,t}$, i.e., a lower forecast skill.

In step 2, the Thomas–Fiering model, a widely used stochastic model of streamflow variability [5,37], is used in synthetic streamflow generation. The model is a first-order autoregressive time series model that can be expressed as

$$q_{t+1} = \mu + \rho_{flow}(q_t - \mu) + \sqrt{1 - \rho_{flow}^2}(\mu C_v)\varepsilon \tag{37}$$

In Eq. (37), μ is the mean value of streamflow, ρ_{flow} is the correlation of streamflow at two consecutive periods, C_v is the coefficient of variation, and ε is a standard Gaussian random number. The mean and variance of streamflow generated by Eq. (37) are μ and $(\mu C_v)^2$, respectively.

There are in total four parameters in Eqs. (36) and (37). The three parameters μ, ρ_{flow}, and C_v in the Thomas–Fiering model (Eq. (37)) are set as constants: $\mu = 1$, $\rho_{flow} = 0.4$, and $C_v = 0.3$. Parameter δ of forecast skill (Eq. (36)) is the control variable in this study. In step 3, for a given streamflow scenario $[q_1, q_2, \ldots, q_{10}]$ simulated via the Thomas–Fiering model, we set $\delta = 0.1$ and generate ensemble forecast with 50 streamflow scenarios ($M = 50$). Ensemble forecast is dynamically updated from periods 1 to 10. The simulated forecast uncertainty is evaluated by the variances of forecast errors at different lead times [23,28,35].

We run 100 Monte Carlo simulations of streamflow sequence and ensemble forecast. The simulated forecast uncertainty is presented by boxplots in Fig. 5. The boxplots illustrate the median as a central mark, the 25th and 75th percentiles as edges, the range of data points as whiskers, and the outliers as plus signs. Moreover, theoretical values of the variances under a specified $CP_{s,t}$, i.e., $(1 - CP_{s,t})^2 \times (qC_v)^2$, are calculated and represented by blue dots linked by a line.

The left side of Fig. 5 illustrates the simulated forecast uncertainty in $f_{1,t}$ ($t = 1, 2, \ldots, 10$) that is formed at period $s = 1$. Larger forecast uncertainty occurred with a longer forecast lead time. This result represents an important characteristic that total predictability and forecast skill of a stochastic system decay with lead time monotonically [7,13]. The right side of Fig. 5 shows forecast uncertainty in dynamically updated $f_{s,10}$ ($s = 1, 2, \ldots, 10$), that is, for q_{10} at period $t = 10$. Forecast uncertainty reduces as time s progresses because forecast skill improves (Eq. (35)). Notably, the simulated magnitudes of forecast uncertainty are in accordance with the theoretical values. As shown in Fig. 5, the FMFE model efficiently simulates the evolution of streamflow forecast.

5. Forecast-based reservoir operation

Streamflow forecast provides useful information on future streamflow and is extensively used in water resource management [9,11,28]. Based on forecasts simulated by the FMFE model, this section presents an analysis of forecast-based decision making. Reservoir operations based on deterministic and ensemble forecasts are compared with reservoir operation under standard operating policy, and effect of forecast skill on forecast-based decision making is analyzed.

5.1. Reservoir operation optimization

Dynamically updated forecasts assist in the rolling-horizon process of decision making. At the beginning of one period, operation decisions are made based on available forecasts, and the current decision is implemented. At the beginning of the next period, forecasts are improved and operation decisions are updated. This process continues until the end of the operation horizon. We incorporate simulated forecasts into the rolling-horizon process and explore the relationship between forecast skill and efficiency of decision making. Three levels of forecast skills are set as follows:

$$\delta = 0.00, 0.10, 0.20 \tag{38}$$

The study horizon T of reservoir operation is set as 10 periods. The Thomas–Fiering model is applied to generate streamflow sequences with the following parameters:

$$\mu = 1.0, \quad \rho_{flow} = 0.4, \quad C_v = 0.3 \tag{39}$$

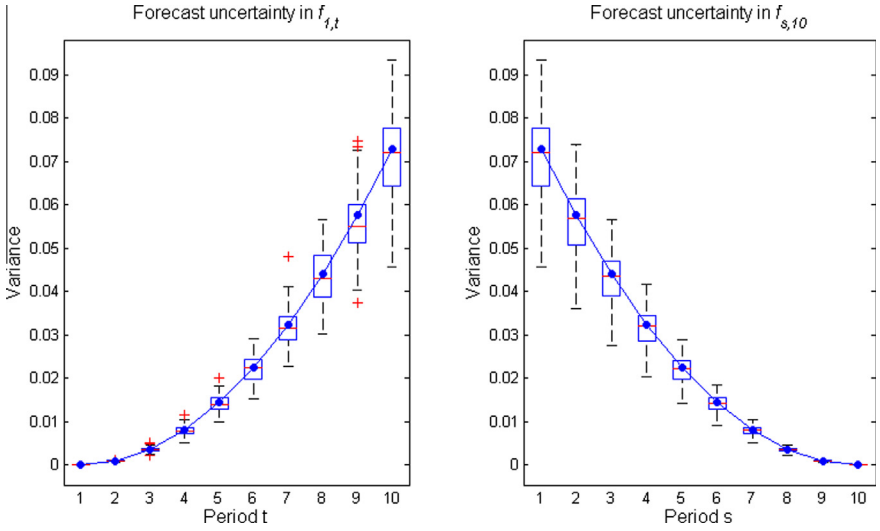

Fig. 5. Evaluation of forecast uncertainty in synthetic forecasts $f_{1,t}$ ($t = 1, 2, \ldots, 10$) and $f_{s,10}$ ($s = 1, 2, \ldots, 10$).

The FMFE model is then applied to simulate dynamically updated deterministic and ensemble forecasts.

The forecast-based reservoir optimization model is formulated as follows:

$$\min \quad \sum_{t=1}^{OH} b_t(r_t)$$
$$s.t. \quad \begin{cases} s_t + x_t - r_t = s_{t+1} & (t = 1,2,\ldots,OH) \\ s_{\min} \leqslant s_t \leqslant s_{\max} & (t = 2,3,\ldots,OH) \\ s_1 = s_{ini} \\ s_{OH+1} = s_{end} \end{cases} \tag{40}$$

In Eq. (40), s_t denotes the reservoir storage at the beginning of period t; and r_t and x_t are reservoir release and forecast of streamflow in period t, respectively. The objective function is cost minimization for the whole operation horizon OH subject to constraints of water balance, storage capacity, and initial and ending storage. In Eq. (40), the minimum storage $s_{\min}$ is set as 0; the maximum storage $s_{\max}$ represents reservoir regulating capacity of streamflow, for which two scenarios are set, namely,

$$S_{\max} = 1,5 \tag{41}$$

To circumvent initial and ending storage effects, s_{ini} and s_{end} are set as $(s_{\min} + s_{\max})/2$. Reservoir operation aims to meet the water demand TD_t. Shortage index SI is set as the single-period objective function

$$b_t(r_t) = SI = \left(\frac{TS_t}{TD_t}\right)^2 \tag{42}$$

In Eq. (42), water shortage $TS_t = \max(0, TD_t - r_t)$. The increase of TS_t incurs an increasing cost of SI. For simplicity, TD_t is set as the mean value of streamflow, i.e., $TD_t = \mu = 1$.

Eqs. (40) and (42) show that reservoir regulates streamflow and aims to minimize the sum of SI within the OH periods. The decisions are based on forecasts that are dynamically updated in the rolling-horizon process. For period 1, $[f_{1,1}, f_{1,2}, \ldots, f_{1,1+OH-1}]$ is used in decision making, as follows:

$$[x_1 \quad x_2 \quad \ldots \quad x_{\text{OH}}] = [f_{1,1} \quad f_{1,2} \quad \ldots \quad f_{1,OH}] \tag{43}$$

Based on Eqs. (40) and (43), r_1^* is derived and implemented. At period 2, forecasts are updated, i.e.,

$$[x_1 \quad x_2 \quad \ldots \quad x_{OH}] = [f_{2,2} \quad f_{2,3} \quad \ldots \quad f_{2,2+OH-1}] \tag{44}$$

Using Eqs. (40) and (44), we determine and implement r_2^*. This process continues until the end of operation at horizon T.

The rolling-horizon process uses dynamically updated forecasts and sequentially determines $r_1^*, r_2^*, \ldots, r_T^*$. The overall SI under forecast-based decision making is derived, as follows:

$$SI = \frac{1}{T}\sum_{t=1}^{T} b_t(r_t^*) \tag{45}$$

The FMFE model simulates deterministic and ensemble streamflow forecasts. The case that applies deterministic forecast to reservoir operation employs dynamic programming to solve Eq. (40), which is denoted by DF-DP; the case that uses ensemble forecast solves Eq. (40) by stochastic dynamic programming, which is denoted by EF-SDP [37,39]. Notably, the optimization models are solved by the improved dynamic programming (IDP) algorithm, which takes advantage of diminishing marginal utility characteristics of reservoir system and improves the computational efficiency of conventional DP [40,41]. As a comparison, standard operating policy (SOP) is used in reservoir operation, which satisfies TD_t when enough water is available, i.e., $s_t + r_t - TD_t > s_{min}$, and spills excess water when $s_t + r_t - TD_t > s_{max}$ [8]. The comparison of DF-DP and EF-SDP to SOP illustrates efficiency of forecast-based decision making.

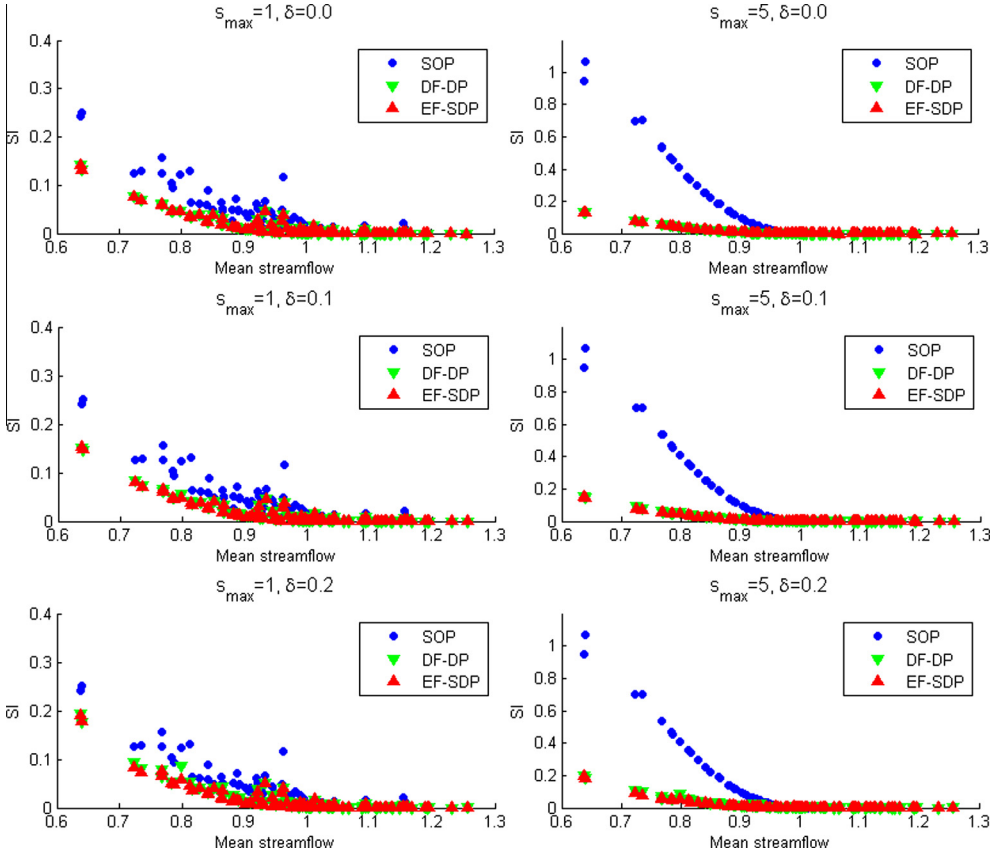

Fig. 6. Relationship between SI and mean streamflow in reservoir operations under SOP, DF-DP, and EF-SDP.

5.2. Effect of forecast skill

We run 100 Monte Carlo simulations for each of the six combinations of δ (Eq. (38)) and s_{max} (Eq. (41)). *SI* under the three cases of reservoir operation are plotted against mean streamflow, i.e., $\frac{1}{T}\sum_{t=1}^{T} q_t$, in Fig. 6. As shown, *SI* reduces as mean streamflow increases because increased streamflow augments water availability to meet water demand. SOP (blue circles) incurs considerable *SI* in reservoir operation, particularly when mean streamflow is low. Compared with SOP, DF-DP (green downward-pointing triangle), and EF-SDP (red upward-pointing triangle) exhibit considerable reduction in *SI*. The result is due to DF-DP and EF-SDP balancing the trade-off between current and future water use based on streamflow forecasts and carrying over water from high-flow periods to low-flow periods, which reduce the overall *SI*. Fig. 6 highlights the effectiveness of forecast-based reservoir operation.

The results in Fig. 6 also illustrate that forecast tends to be more valuable for reservoirs with larger storage capacity. As shown, SOP under $s_{max} = 5$ leads to larger *SI* than SOP under $s_{max} = 1$ because SOP satisfies current demand regardless of future use [8]. When streamflow is limited, reservoir storage is depleted from the initial storage until reservoir storage reaches the lower bound; depleted storage incurs considerable shortage at the end of the study horizon, inducing drastic *SI* (Eq. (42)). Conversely, forecast-based reservoir operation significantly reduces *SI*. When $\delta = 0$, i.e., perfect forecast, *SI* is decreased by increased mean streamflow under $s_{max} = 5$; whereas *SI* is not always reduced by increased mean streamflow under $s_{max} = 1$. When $\delta = 0.1$ and $\delta = 0.2$, the reducing effect of mean streamflow on *SI* is stronger under $s_{max} = 5$ than under $s_{max} = 1$. Larger s_{max} allows reservoir regulation of streamflow at a longer timeframe and enables more efficient use of forecast in decision making.

5.3. Effect of operation horizon

In Section 5.2, the simulations consider operation horizon as the remaining study horizon (i.e., *OH* is *T* at period 1, $T-1$ at period 2, and so on). This setting provides the maximum forecast information for decision making. Meanwhile, forecast at a longer lead time involves larger uncertainty, which can reduce the efficiency of decision making. To explore the trade-offs between "more but less reliable" and "less but more certain" forecast information, this section simulates reservoir operation with different *OH* settings. For example, when *OH* is set as 2, the decision r_s^* at period *s* is based on $[f_{s,s}, f_{s,s+1}]$ instead of forecasts $[f_{s,s}, f_{s,s+1}, \ldots, f_{s,T}]$ for the remaining study horizon. By varying *OH* from 2 to 10 periods, we conduct 100 Monte Carlo simulations for each *OH* and evaluate the corresponding *SI*. Figs. 7 and 8 illustrate the relationship between *SI* and *OH* under $s_{max} = 1$ and $s_{max} = 5$, respectively.

The left- and right-hand sides of the figures compare reservoir operations under deterministic and ensemble forecasts. $\delta = 0$ represents perfect forecast without forecast uncertainty. In this case, deterministic and ensemble forecasts are equivalent, which leads to a similar *SI* in reservoir operation. When $\delta = 0.1$ and $\delta = 0.2$, decision making is subject to forecast uncertainty. In the two cases, ensemble forecast leads to a more efficient reservoir operation than deterministic forecast does with regard to smaller mean value and standard deviation for *SI*. The efficiency improvement is attributed to the ensemble forecast containing multiple scenarios and providing more reliable characterization of forecast uncertainty [9,23,35].

As indicated by the mean value and standard deviation of *SI* at different *OHs*, longer *OH* allows for use of more forecast information but does not necessarily contribute to reservoir operation. When $\delta = 0$, forecast is perfect, and increase of *OH* leads to reduction of the mean value and standard deviation of *SI*. However, when $\delta = 0.1$ or $\delta = 0.2$, *SI* depends on both *OH* and δ. If *OH* is short, then the mean value and standard deviation of *SI* decrease with increased *OH*. However, a threshold for *OH* is present beyond which mean value and standard deviation of *SI* can even increase with increased *OH*. Zhao et al. [38] described the threshold as effective forecast horizon (EFH) and illustrated that efficiency of decision making is dominated by forecast uncertainty when using forecast information beyond EFH. Figs. 7 and 8 show that EFH exists in both deterministic and ensemble forecasts and that EFH is reduced by increased δ. Thus, smaller forecast skill and larger forecast uncertainty lead to shorter EFH. Moreover, EFH increases as s_{max} increases from 1 to 5 because large reservoirs can regulate

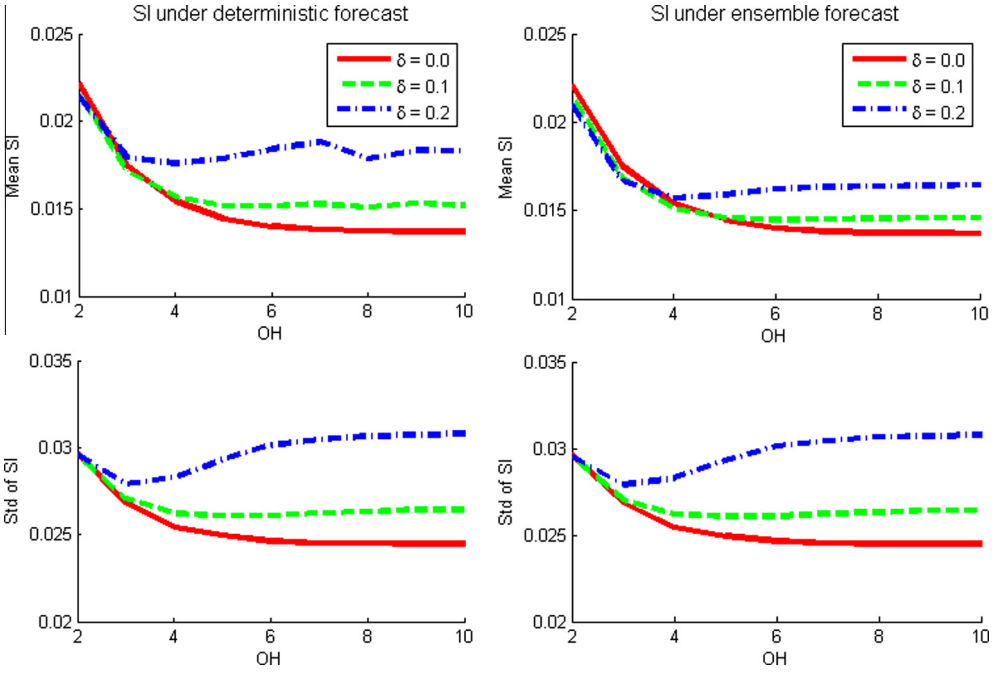

Fig. 7. Shortage index under forecast-based reservoir operation with different operation horizons ($s_{max} = 1$).

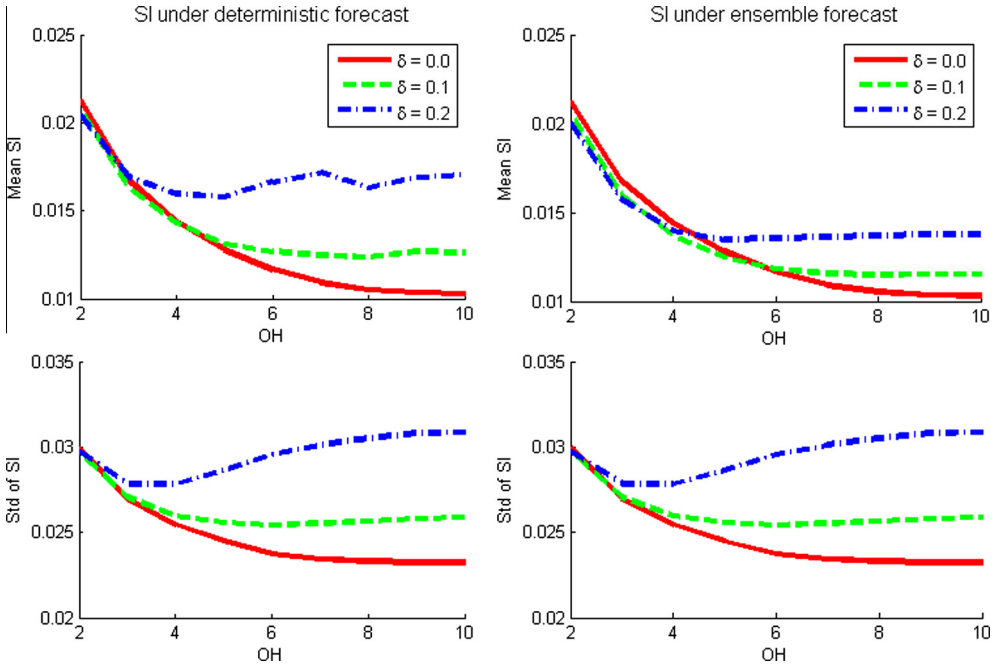

Fig. 8. Shortage index under forecast-based reservoir operation with different operation horizons (s_{max} = 5).

streamflow at a long timeframe and require more forecast information [38].

6. Discussions and conclusions

Streamflow forecasts are updated periodically in real-time cases. Forecast uncertainty increases with forecast lead time. Meanwhile, uncertainty of streamflow in one future period decreases as time progresses and more hydrological data become available. This study proposes the FMFE model based on stochastic models for synthetic streamflow generation and extends the models to synthetic forecast generation by incorporating coefficients of prediction, which account for forecast skills. Generally, streamflow scenarios generated by stochastic models represent cases without forecast skill. Coefficients of prediction represent the ratio of streamflow variability explained by the forecast that results from the forecast skill. By updating coefficients of prediction periodically, the FMFE model simulates the dynamic evolution of streamflow forecast.

We combine the FMFE model with an optimization model and present an analysis of forecast-based decision making. The results show that shortage index reduces as forecast skill increases and that ensemble forecast outperforms deterministic forecast at a similar forecast skill level. Moreover, an effective forecast horizon exists beyond which more forecast information does not contribute to reservoir operation. Higher forecast skill provides more reliable forecast information and results in longer effective forecast horizon. The significance of forecast skill illustrates the importance of improving streamflow forecast to decision making. The FMFE model simulates streamflow forecast based on forecast skill and facilitates an effective approach to analyzing forecast-based decision making.

Forecast uncertainty closely relates to streamflow variability that depends on climate and landscape attributes [4]. Forecast uncertainty is also affected by initial hydrological conditions, atmospheric forcing, as well as structures and parameters of the hydrological model [9,19,28]. In real-world cases, forecast uncertainty can be highly complex. For example, although total predictability of a stochastic system decays with time [7], predictability of certain components in the system can rebound because of interactions among the components [13]. The current study builds the linkage between streamflow variability and forecast uncertainty via forecast skill, therefore developing the FMFE model for simulation of streamflow forecasts. Future studies should closely investigate the relationship between streamflow variability and forecast uncertainty to provide a more solid physical basis for the FMFE model.

Acknowledgments

We are grateful to the Editor and the two anonymous reviewers for their constructive suggestions, which have facilitated major improvements in this paper. This research was supported by the Ministry of Science and Technology of China (Project No. 2011BAC09B07 and No. 2013BAB05B03), the National Natural Science Foundation of China (Project No. 51179085), and the China Postdoctoral Science Foundation (Project No. 2014M550071).

References

[1] Ajami NK, Duan QY, Sorooshian S. An integrated hydrologic Bayesian multimodel combination framework: confronting input, parameter, and model structural uncertainty in hydrologic prediction. Water Resour Res 2007;43(1). http://dx.doi.org/10.1029/2005wr004745.
[2] Ajami NK, Hornberger GM, Sunding DL. Sustainable water resource management under hydrological uncertainty. Water Resour Res 2008;44(11). http://dx.doi.org/10.1029/2007wr006736.
[3] Bavay M, Grunewald T, Lehning M. Response of snow cover and runoff to climate change in high Alpine catchments of Eastern Switzerland. Adv Water Resour 2013;55:4–16. http://dx.doi.org/10.1016/j.advwatres.2012.12.009.
[4] Botter G, Basso S, Rodriguez-Iturbe I, Rinaldo A. Resilience of river flow regimes. Proc Nat Acad Sci USA 2013;110(32):12925–30. http://dx.doi.org/10.1073/pnas.1311920110.
[5] Booker JF, O'Neill JC. Can reservoir storage be uneconomically large? J Water Resour Planning Manage – ASCE 2006;132(6):520–3. http://dx.doi.org/10.1061/(asce)0733-9496(2006)132:6(520).
[6] Carvajal C, Peyras L, Arnaud P, Boissier D, Royet P. Probabilistic modeling of floodwater level for dam reservoirs. J Hydrol Eng 2009;14(3):223–32. http://dx.doi.org/10.1061/(asce)1084-0699(2009)14:3(223).
[7] Cover TM, Thomas JA. Elements of information theory. Wiley-Interscience; 1991. p. 542.

[8] Draper A, Lund J. Optimal hedging and carryover storage value. J Water Resour Planning Manage 2004;130(1):83–7. http://dx.doi.org/10.1061/(asce)0733-9496(2004)130:1(83).
[9] Georgakakos AP, Yao H, Kistenmacher M, Georgakakos KP, Graham NE, Cheng FY, Spencer C, Shamir E. Value of adaptive water resources management in Northern California under climatic variability and change: reservoir management. J Hydrol 2012;412:34–46. http://dx.doi.org/10.1016/j.jhydrol.2011.04.038.
[10] Georgakakos KP, Graham NE. Potential benefits of seasonal inflow prediction uncertainty for reservoir release decisions. J Appl Meteorol Climatol 2008;47(5):1297–321. http://dx.doi.org/10.1175/2007jamc1671.1.
[11] Georgakakos KP, Graham NE, Cheng FY, Spencer C, Shamir E, Georgakakos AP, Yao H, Kistenmacher M. Value of adaptive water resources management in northern California under climatic variability and change: dynamic hydroclimatology. J Hydrol 2012;412:47–65. http://dx.doi.org/10.1016/j.jhydrol.2011.04.032.
[12] Graham NE, Georgakakos KP. Toward understanding the value of climate information for multiobjective reservoir management under present and future climate and demand scenarios. J Appl Meteorol Climatol 2010;49(4):557–73. http://dx.doi.org/10.1175/2009jamc2135.1.
[13] Guo ZC, Dirmeyer PA, DelSole T, Koster RD. Rebound in atmospheric predictability and the role of the land surface. J Clim 2012;25(13):4744–9. http://dx.doi.org/10.1175/jcli-d-11-00651.1.
[14] Heath DC, Jackson PL. Modeling the evolution of demand forecasts with application to safety stock analysis in production distribution-systems. IIE Trans 1994;26(3):17–30. http://dx.doi.org/10.1080/07408179408966604.
[15] Ilich N, Despotovic J. A simple method for effective multi-site generation of stochastic hydrologic time series. Stochastic Environ Res Risk Assess 2008;22(2):265–79. http://dx.doi.org/10.1007/s00477-007-0113-6.
[16] Kelly KS, Krzysztofowicz R. A bivariate meta-Gaussian density for use in hydrology. Stochastic Hydrol Hydraulics 1997;11(1):17–31. http://dx.doi.org/10.1007/bf02428423.
[17] Labadie JW. Optimal operation of multireservoir systems: state-of-the-art review. J Water Resour Planning Manage – ASCE 2004;130(2):93–111. http://dx.doi.org/10.1061/(asce)0733-9496(2004)130:2(93).
[18] Lall U, Sharma A. A nearest neighbor bootstrap for resampling hydrologic time series. Water Resour Res 1996;32(3):679–93. http://dx.doi.org/10.1029/95wr02966.
[19] Li HB, Luo LF, Wood EF, Schaake J. The role of initial conditions and forcing uncertainties in seasonal hydrologic forecasting. J Geophys Res – Atmos 2009;114. http://dx.doi.org/10.1029/2008JD010969.
[20] Li XA, Guo SL, Liu P, Chen GY. Dynamic control of flood limited water level for reservoir operation by considering inflow uncertainty. J Hydrol 2010;391(1–2):126–34. http://dx.doi.org/10.1016/j.jhydrol.2010.07.011.
[21] Loucks DP, van Beek E. Water resources systems planning and management: an introduction to methods, models and applications. UNESCO, Paris; 2005.
[22] Maurer EP, Lettenmaier DP. Predictability of seasonal runoff in the Mississippi River basin. J Geophys Res – Atmos 2003;108(D16). http://dx.doi.org/10.1029/2002jd002555.
[23] Maurer EP, Lettenmaier DP. Potential effects of long-lead hydrologic predictability on Missouri River main-stem reservoirs. J Clim 2004;17(1):174–86. http://dx.doi.org/10.1175/1520-0442(2004)017<0174:peolhp>2.0.co;2.
[24] Montanari A. Deseasonalisation of hydrological time series through the normal quantile transform. J Hydrol 2005;313(3–4):274–82. http://dx.doi.org/10.1016/j.jhydrol.2005.03.008.
[25] Prairie JR, Rajagopalan B, Fulp TJ, Zagona EA. Modified K-NN model for stochastic streamflow simulation. J Hydrol Eng 2006;11(4):371–8. http://dx.doi.org/10.1061/(asce)1084-0699(2006)11:4(371).
[26] Salas JD, Sveinsson OG, Lane WL, Frevert DK. Stochastic streamflow simulation using SAMS-2003. J Irrigation Drainage Eng – Asce 2006;132(2):112–22. http://dx.doi.org/10.1061/(asce)0733-9437(2006)132:2(112).
[27] Samuel J, Coulibaly P, Metcalfe RA. Evaluation of future flow variability in ungauged basins: validation of combined methods. Adv Water Resour 2012;35:121–40. http://dx.doi.org/10.1016/j.advwatres.2011.09.015.
[28] Sankarasubramanian A, Lall U, Devineni N, Espinueva S. The role of monthly updated climate forecasts in improving intraseasonal water allocation. J Appl Meteorol Climatol 2009;48(7):1464–82. http://dx.doi.org/10.1175/2009jamc2122.1.
[29] Shi XG, Wood AW, Lettenmaier DP. How essential is hydrologic model calibration to seasonal streamflow forecasting? J Hydrometeorol 2008;9(6):1350–63. http://dx.doi.org/10.1175/2008jhm1001.1.
[30] Srinivas VV, Srinivasan K. Hybrid matched-block bootstrap for stochastic simulation of multiseason streamflows. J Hydrol 2006;329(1–2):1–15. http://dx.doi.org/10.1016/j.jhydrol.2006.01.023.
[31] Tarboton DG, Sharma A, Lall U. Disaggregation procedures for stochastic hydrology based on nonparametric density estimation. Water Resour Res 1998;34(1):107–19. http://dx.doi.org/10.1029/97wr02429.
[32] Vicuna S, Dracup JA, Lund JR, Dale LL, Maurer EP. Basin-scale water system operations with uncertain future climate conditions: methodology and case studies. Water Resour Res 2010;46:W04505. http://dx.doi.org/10.1029/2009WR007838.
[33] Vogel RM, Stedinger JR. The value of stochastic streamflow models in overyear reservoir design applications. Water Resour Res 1988;24(9):1483–90. http://dx.doi.org/10.1029/wr024i009p01483.
[34] Wei WW, Watkins DW. Data mining methods for hydroclimatic forecasting. Adv Water Resour 2011;34(11):1390–400. http://dx.doi.org/10.1016/j.advwatres.2011.08.001.
[35] Weigel AP, Liniger MA, Appenzeller C. Can multi-model combination really enhance the prediction skill of probabilistic ensemble forecasts? Q J R Meteorol Soc 2008;134(630):241–60. http://dx.doi.org/10.1002/qj.210.
[36] Wood AW, Lettenmaier DP. An ensemble approach for attribution of hydrologic prediction uncertainty. Geophys Res Lett 2008;35(14). http://dx.doi.org/10.1029/2008gl034648.
[37] Zhao TTG, Cai XM, Yang DW. Effect of streamflow forecast uncertainty on real-time reservoir operation. Adv Water Resour 2011;34(4):495–504. http://dx.doi.org/10.1016/j.advwatres.2011.01.004.
[38] Zhao TTG, Yang DW, Cai XM, Zhao JS, Wang H. Identifying effective forecast horizon for real-time reservoir operation under a limited inflow forecast. Water Resour Res 2012;48. http://dx.doi.org/10.1029/2011WR010623.
[39] Zhao TTG, Zhao JS, Yang DW, Wang H. Generalized martingale model of the uncertainty evolution of streamflow forecasts. Adv Water Resour 2013;57:41–51. http://dx.doi.org/10.1016/j.advwatres.2013.03.008.
[40] Zhao TTG, Cai XM, Lei XH, Wang H. Improved dynamic programming for reservoir operation optimization with concave utility functions. J Water Resour Planning Manage – ASCE 2012;138(6):590–6. http://dx.doi.org/10.1061/(asce)wr.1943-5452.0000205.
[41] Zhao TTG, Zhao JS, Yang DW. Improved dynamic programming for hydropower reservoir operation. J Water Resour Planning Manage – ASCE 2014;140(3):365–74. http://dx.doi.org/10.1061/(asce)wr.1943-5452.0000343.